

# JGR Space Physics

## RESEARCH ARTICLE

10.1029/2021JA029669

### Key Points:

- Magnetospheric Multiscale (MMS) encounters the magnetopause reconnection site over a wide range of external conditions
- The occurrence of reconnection region encounters is consistent with that of large-scale magnetopause motion, and depends on interplanetary magnetic field orientation
- Distributions of MMS locations with respect to model reconnection line predictions are independent of region downstream of the bow shock

### Correspondence to:

S. M. Petrinec,  
[petrinec@lmsal.com](mailto:petrinec@lmsal.com)

### Citation:

Petrinec, S. M., Burch, J. L., Fuselier, S. A., Trattner, K. J., Giles, B. L., & Strangeway, R. J. (2022). On the occurrence of magnetic reconnection along the terrestrial magnetopause, using Magnetospheric Multiscale (MMS) observations in proximity to the reconnection site. *Journal of Geophysical Research: Space Physics*, 127, e2021JA029669. <https://doi.org/10.1029/2021JA029669>







Received 13 JUN 2021  
Accepted 14 MAY 2022

### Author Contributions:

**Conceptualization:** S. M. Petrinec, S. A. Fuselier  
**Data curation:** J. L. Burch, S. A. Fuselier, B. L. Giles, R. J. Strangeway  
**Formal analysis:** S. M. Petrinec  
**Investigation:** S. M. Petrinec, J. L. Burch, S. A. Fuselier, K. J. Trattner  
**Methodology:** S. M. Petrinec  
**Resources:** S. A. Fuselier, B. L. Giles, R. J. Strangeway  
**Writing – original draft:** S. M. Petrinec

© 2022. American Geophysical Union. All Rights Reserved.  
This is an open access article under the terms of the [Creative Commons Attribution-NonCommercial-NoDerivs License](https://creativecommons.org/licenses/by-nc-nd/4.0/), which permits use and distribution in any medium, provided the original work is properly cited, the use is non-commercial and no modifications or adaptations are made.

## On the Occurrence of Magnetic Reconnection Along the Terrestrial Magnetopause, Using Magnetospheric Multiscale (MMS) Observations in Proximity to the Reconnection Site

S. M. Petrinec<sup>1</sup> , J. L. Burch<sup>2</sup> , S. A. Fuselier<sup>2,3</sup> , K. J. Trattner<sup>4</sup> , B. L. Giles<sup>5</sup> , and R. J. Strangeway<sup>6</sup> 

<sup>1</sup>Lockheed Martin Advanced Technology Center, Palo Alto, CA, USA, <sup>2</sup>Southwest Research Institute, San Antonio, TX, USA, <sup>3</sup>University of Texas at San Antonio, San Antonio, TX, USA, <sup>4</sup>University of Colorado, Boulder, CO, USA, <sup>5</sup>NASA Goddard Space Flight Center, Greenbelt, MD, USA, <sup>6</sup>University of California, Los Angeles, CA, USA

**Abstract** Observations at the reconnection site from the Magnetospheric Multiscale mission are used to examine the occurrence of magnetic reconnection along the magnetopause in relation to both the upstream interplanetary magnetic field (IMF) orientation and local magnetosheath variations. While there is a statistically larger number of reconnection intervals observed downstream of the quasi-parallel bow shock than is accounted for based on the histogram of overall IMF orientations, it is surmised that increased fluctuations downstream of the quasi-parallel bow shock cause greater large-scale motion of the magnetopause surface; but do not preferentially enhance the occurrence of steady magnetic reconnection. An examination of the locations of observed reconnection sites relative to model predictions also suggest that enhanced magnetosheath fluctuations do not result in steady reconnection occurring at random locations at the magnetopause.

## 1. Introduction

Magnetic reconnection is recognized as the primary process by which bulk solar wind plasma enters the magnetosphere. Over the past several decades, there have been many direct and indirect observations of magnetic reconnection at the terrestrial magnetopause by sampling spacecraft. Indirect observations are varied, and include the inward (earthward) motion of the magnetopause in response to an extended interval of southward interplanetary magnetic field (IMF) (Aubry et al., 1970), in situ observations of accelerated ion flows tangent to the magnetopause and within the boundary layers (e.g., Gosling et al., 1982, 1986; Gosling et al., 1990a, 1990b; Lavraud et al., 2005; Paschmann et al., 1989; Petrinec et al., 2016; Phan et al., 2000; Scurry et al., 1994; Sonnerup et al., 1981; Trattner et al., 2012; Trenchi et al., 2008; Vines et al., 2015), observations of cusp ion energy dispersions (e.g., Escoubert et al., 1992; Newell & Meng, 1991; Reiff et al., 1977; Rosenbauer et al., 1975; Shelley et al., 1976; Trattner et al., 1999), and imaging of cusp ionosphere emissions due to particle precipitation from the magnetopause (e.g., Bobra et al., 2004; Frey et al., 2002, 2003; Fuselier et al., 2002; Phan et al., 2003). Recently, direct multi-point observations of the reconnection process within the ion and electron diffusion regions (EDRs) have been made by the Magnetospheric Multiscale (MMS) mission (Burch et al., 2016; Webster et al., 2018). These observations have provided fundamental insights into the microphysics of magnetic reconnection of collisionless plasmas.

The overall amount of plasma and energy transport across the magnetopause is affected by the reconnection rate along the reconnection line as well as the spatial extent of the reconnection line. These parameters are in turn influenced by parameters such as the orientation of the IMF, the local change in plasma beta between the magnetosheath and magnetosphere, the velocity shear across the magnetopause boundary, and minor ion abundances.

For steady solar wind conditions, magnetic reconnection at the magnetopause is generally believed to be steady; characterized by a non-zero—and perhaps constant—reconnection rate. Steady reconnection during intervals of steady southward IMF at the magnetopause is thought to occur along continuous reconnection line(s) extending across a considerable span of local time along the magnetopause surface, at low- to mid-latitudes (Trattner, Petrinec, & Fuselier, 2021, and references therein). Although the extent of the steady reconnection line is not well quantified, it is expected that various parameters influence whether magnetic reconnection at a particular location on the magnetopause can be steady, unsteady, or not possible (e.g., Cowley & Owen, 1989). Such parameters include the local magnetic shear angle across the magnetopause (e.g., Crooker, 1979; Gonzalez & Mozer, 1974;

**Writing – review & editing:** J. L. Burch, S. A. Fuselier, K. J. Trattner, B. L. Giles, R. J. Strangeway

Luhmann et al., 1984; Trattner et al., 2007), the change in plasma beta ( $\Delta\beta$ ) across the magnetopause (e.g., Fuselier et al., 2014, 2020; Masters et al., 2012; Swisdak et al., 2003), and the magnetosheath Mach number (and related velocity shear (e.g., Desroche et al., 2012, 2013; Doss et al., 2015; Petrínek et al., 2003; Sawyer et al., 2019)).

The inferred existence of extended reconnection lines at the magnetopause from in situ observations is quite limited, because sampling spacecraft cross the boundary at a single location at a single time. As described in a study of accelerated ion flows observed during multiple magnetopause crossings as compiled from the International Sun-Earth Explorers (ISEE-1/2) mission by Scurry et al. (1994), the local time extent of the reconnection line cannot be reliably estimated solely from single-point observations at the magnetopause. Observational evidence of extended reconnection lines thus requires simultaneous in situ observations at multiple magnetopause locations. In one published case, simultaneous observations of reconnection from two widely spaced spacecraft at low latitudes along the flank magnetopause was consistent with a reconnection line of at least  $3 R_E$  in extent (Phan et al., 2000). Dunlop et al. (2011) used a conjunction of 10 spacecraft encountering the magnetopause to demonstrate that a reconnection line may extend over nearly the entire dayside magnetopause.

Ion observations from sampling spacecraft within the cusp region at lower altitudes provide remote signatures of the occurrence of reconnection at the magnetopause (cf., Smith & Lockwood, 1996; Trattner et al., 1998), and this also provides information as to the location of reconnection lines (Trattner et al., 2005, 2007; Trattner, Petrínek, & Fuselier, 2021). Further, the precipitation of plasma into the high-latitude (i.e., cusp) ionosphere produces emissions that can be observed from space (e.g., using global auroral imagers such as provided by the IMAGE/FUV instrument (Fuselier et al., 2002)), providing information as to the extent of reconnection at the magnetopause.

These disparate sets of observations have provided compelling evidence for the presence of extended reconnection lines along the dayside magnetopause, and strongly suggest that such reconnection lines are persistent during intervals of steady IMF and solar wind plasma conditions (e.g., Frey et al., 2003).

In addition to the orientation of the IMF and variations in plasma parameters within the solar wind, plasma waves and turbulence initiated at the standing bow shock and within the magnetosheath enhance fluctuations that can potentially reach the magnetopause. It has been questioned whether the effect of such magnetosheath fluctuations impacting the magnetopause could influence the occurrence of magnetic reconnection at the magnetopause (e.g., Hietala et al., 2018; Russell et al., 1997; Scurry & Russell, 1991). A change in the occurrence of reconnection should be observable during times when the IMF is steady and slightly northward, with magnetosheath fluctuations of southward magnetic field impacting the dayside magnetopause. This scenario has been proposed to initiate transient reconnection associated with flux transfer events (FTEs) (Sibeck, 1992). However, this has generally not been observed in relation to FTE occurrence (Kawano & Russell, 1996). In addition, the location of the subsolar magnetopause is unaffected by brief intervals of southward magnetosheath magnetic field when the IMF is northward (Zhang et al., 1997). Rather than observing a relative increase in the initiation of reconnection during intervals of southward magnetic fields, an increased number of magnetopause oscillations as well as oscillation amplitude of the magnetopause has been observed (Russell et al., 1997; Song et al., 1988).

It has been well-understood that a variety of wave phenomena and turbulence are initiated either at the bow shock and/or within the magnetosheath, producing significant fluctuations in field and plasma parameters over a wide range of time scales, from frequencies above  $\sim 0.01$  Hz (e.g., Li et al., 2020) to frequencies below  $\sim 0.1$  Hz (e.g., Gutynska et al., 2012; Schwartz et al., 1996). These fluctuations arise from several different physical processes occurring both at the bow shock and within the magnetosheath (Schwartz et al. (1996); Li et al. (2020), and references therein), and could potentially influence phenomena at the magnetopause and within the magnetosphere (Fairfield & Ness, 1970). The effectiveness of some of these processes in creating plasma fluctuations is dependent on the angle of the IMF with respect to the standing bow shock normal direction. The “quasi-parallel” region of the bow shock (where the angle  $\theta_{\text{Bn}} = \cos^{-1}(|\mathbf{B}_{\text{IMF}} \cdot \mathbf{n}_{\text{BS-out}}|/B_T)$  is  $< 45^\circ$ , and  $\mathbf{n}_{\text{BS-out}}$  represents the outward unit normal of the bow shock surface, and  $B_T$  is the IMF intensity) is known to be a region of enhanced fluctuations in the magnetic field and plasma moments (particularly density); primarily from the initiation and propagation of waves by backstreaming ions downstream of the (ion) foreshock. These waves then convect across the bow shock into the magnetosheath mainly along plasma streamlines, in addition to shock reformation processes.

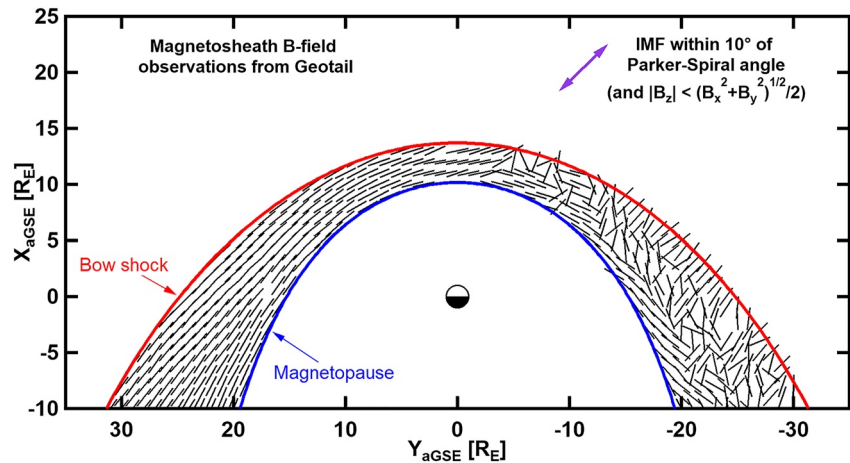


**Figure 1.** Binned Geotail 5-min resolution observations of median magnetosheath magnetic field orientation (April 1996–October 2005), during times of nominal Parker spiral angle. Interplanetary magnetic field conditions while Geotail was in the magnetosheath were determined from convected Wind magnetic field observations. See Petrínek, 2013 for additional description of data set.

Fluctuations in the magnetosheath region downstream of the quasi-perpendicular region of the bow shock are of relatively smaller amplitude when compared to the region downstream of the quasi-parallel shock.

Plasma streamlines close to the Sun–Earth line are those that stream closest to the magnetopause, and are sometimes described as “painting” the magnetopause (cf., Russell (2002)). As a consequence, fluctuations resulting from quasi-parallel or quasi-perpendicular bow shock effects at the magnetopause are typically described in terms of the IMF orientation relative to the Sun–Earth line, or IMF “cone angle.” Although pressure fluctuations generated along part of the bow shock surface and within the magnetosheath may convect across streamlines, the IMF “cone angle” is a reasonable metric to ascertain whether regions of the magnetopause surface are downstream of the quasi-parallel or quasi-perpendicular bow shock. Depending on usage, the IMF “cone angle” definition can be ambiguous. Here (and throughout the remainder of this manuscript) the IMF “cone angle” is defined as follows:  $\text{cone\_angle} = \theta_{B_x} = \cos^{-1}(|B_x|/B_T) \{0^\circ \leq \theta_{B_x} \leq 90^\circ\}$ ;  $\text{cone\_angle}_2 = \theta_{B_{x2}} = \cos^{-1}(B_x/B_T) \{0^\circ \leq \theta_{B_{x2}} \leq 180^\circ\}$ .

Luhmann et al. (1986) performed a statistical study of ISEE-2 observations throughout the magnetosheath when IMP-8 was in the solar wind. In their study, both compressional and transverse fluctuations in the magnetic field were investigated as a function of both IMF cone\_angle and local time. The fluctuations were shown to be statistically largest when the angle between the IMF and the Sun–Earth line ( $\theta_{B_x}$  normal to the surface of the bow shock at the subsolar location) was small, with the largest fluctuations closer to local noon than at local times closer to dawn or dusk. The contrast between smallest and largest fluctuation levels was about a factor of 2, though with a significant “typical error.” Němeček et al. (2000) used Interball observations in the magnetosheath, solar wind, and foreshock to determine that magnetosheath fluctuations are present whenever the IMF cone\_angle was  $<40^\circ$ , independent of the local  $\theta_{B_n}$ —implicating the subsolar foreshock as the source of the fluctuations. Shevryev et al. (2003) analyzed a few dozen magnetosheath flank passes by INTERBALL-1 and IMP 8 with solar wind observations from Wind for upstream context. This analysis revealed an increased amplitude of variations in both the ion flux and magnetic field intensity in the flank magnetosheath region relative to the solar wind (by a factor of 2–3 times), at both high frequencies (wave periods of several to tens of seconds) and low frequencies (wave periods of several to tens of minutes). A marked dependence of wave activity on  $\theta_{B_n}$  was also noted within the magnetosheath, similar to that shown by Luhmann et al. (1986). A notable difference in magnetosheath magnetic field vector fluctuations when the IMF was close to the Parker spiral angle ( $\theta_{B_x} (= \theta_{B_n}$  at bow shock nose) =  $45 \pm 10^\circ$ ) is illustrated in Figure 1 (see Petrínek (2013) for additional description). This statistical study used spatially binned Geotail magnetic field observations within the magnetosheath to show the variability in magnetic field directions within the magnetosheath (medians of Geotail magnetic field unit vectors were determined for each spatial bin). A clear difference between the more ordered dusk side and the more disordered dawn side magnetosheath is evident.

One thing to note from inspection of Figure 1 is that the magnetic field in the dawn magnetosheath does not appear disordered near the magnetopause. Certainly, the magnetic field drapes tangent to the magnetopause surface. However, there may be variations in the magnetic field that are not readily observable in such a presentation. Specifically, there may be transverse fluctuations tangent to the magnetopause but out of the plane of this image. There may also be increased compressional fluctuations within the inner magnetosheath. This then leads to the question of what type of magnetosheath fluctuations actually reach the magnetopause, and under what upstream conditions.

Of the many types of plasma waves and turbulence generated and observed at the bow shock and within the magnetosheath proper, it is of interest for this study to understand whether such variations reach the magnetopause, whether there are significant dependences on IMF orientation and corresponding local time variation along the magnetopause, and whether any such incident fluctuations influence the occurrence and location of magnetopause reconnection. Anderson et al. (1982) described several types of high and low frequency magnetic field and density fluctuations that were observed during a single pass of ISEE-1 from the magnetosheath across the magnetopause and into the outer magnetosphere. Identification of significant wave activity in the inner magnetosheath was described by Song et al. (1992, 1993, 1994) using ISEE plasma and magnetic field observations, and by Denton et al. (1995) using Active Magnetospheric Particle Tracer Explorers/Ion Release Module (AMPTE/IRM) plasma and magnetic field observations. Shevryev et al. (2003) examined both the standard deviation (SD) and the relative (normalized) standard deviation (RSD) of high frequency and low frequency fluctuations of plasma flux along radial profiles between the bow shock and magnetopause, noting that the fluctuations remain constant (SD) throughout the magnetosheath or increase (RSD) nearer the magnetopause than nearer the bow shock. Russell et al. (1983) correlated ground-based observations of PC 3,4 waves within the dayside magnetosphere to the IMF cone\_angle to show both the strong  $\theta_{B_x}$  ( $=\theta_{B_n}$  at bow shock nose) dependence on the occurrence of these coherent low-frequency waves, and that fluctuations resulting from the quasi-parallel bow shock region permeate the magnetosheath and are capable of interacting directly with the magnetopause and magnetosphere magnetic field. Russell et al. (1997) examined ISEE magnetopause crossings (number of crossings per pass and magnetopause oscillation amplitude) as a function of IMF clock angle ( $=\tan^{-1}(B_{yGSM}/B_{zGSM})$ ) and local time. The oscillations in this study referred to changes in the magnetopause location (i.e., magnetopause motion), and did not discern any particular type of motion (incoherent or turbulent fluctuations, coherent surface wave oscillations or resonant wave modes). Overall, more numerous magnetopause crossings with larger oscillation amplitude were observed in the pre-noon sector as compared to the post-noon sector, as would be expected if foreshock pressure fluctuations (during a statistically commonly occurring Parker spiral IMF orientation) were convected to the magnetopause. This was the case for each IMF clock angle bin, suggesting that dayside reconnection during southward IMF conditions was neither enhanced nor inhibited by convected fluctuations from the foreshock to the magnetopause.

Finally, an empirical study of dayside magnetosheath magnetic field fluctuations between 0.1 and 2 Hz using THEMIS observations was conducted by Dimmock et al. (2014). It was found that while fluctuations were larger downstream of the quasi-parallel bow shock (dawn side) in comparison to the quasi-perpendicular bow shock (dusk side), this asymmetry disappeared when the IMF had a southward component. Magnetosheath fluctuations were found, however, to increase in amplitude close to the magnetopause during intervals of southward IMF; and were attributed to processes occurring at the magnetopause under such conditions.

The purpose of this study is to examine in a statistical manner whether such temporal variations in the magnetosheath attributed to plasma waves, fluctuations, and/or turbulence initiated at the bow shock or within the magnetosheath reach the magnetopause and if so, whether they have any effect (i.e., enhancement, suppression, or no effect) on the occurrence of observed steady reconnection at the magnetopause. This determination is to be made by examining whether conditions resulting in enhanced/inhibited magnetosheath wave activity and/or turbulence near the magnetopause is correlated with the occurrence of observed accelerated flows tangent to the magnetopause, or with the occurrence of observed EDRs. The intervals used in this study are limited to those for which the spacecraft is in proximity to the reconnection site; as determined by either the observance of ion jet reversals or the direct sampling of the EDR. This selection criterion reduces any ambiguity that would be caused by the reconnection site being located at a location remote from the sampling spacecraft; with significantly different conditions from that at the sampling spacecraft.

This paper is laid out as follows: Section 2 describes the spacecraft instrument data sets utilized in this study. Section 3 presents a detailed description of two example observational intervals of magnetopause reconnection occurring along the magnetopause flanks, as determined from accelerated flows tangent to the boundary. Section 4 then presents a statistical study of the occurrence of magnetopause reconnection, with particular attention to the distribution of the IMF. The observed location of reconnection relative to the predicted location from the maximum magnetic shear model is also examined in a statistical manner. Section 5 summarizes the results of this investigation.

## 2. Instrumentation/Data Sets Used in Study

The MMS mission was launched in March 2015, with the goal of using the near-Earth environment as a natural laboratory to study collisionless magnetic reconnection (Burch et al., 2016); with primary focus on the magnetopause and the magnetotail neutral sheet. The four-spacecraft constellation completed two sweeps of the dayside magnetopause from the dusk to dawn flanks (each sweep comprising several dozen orbits) during the first 2 years of science operations. During these two sweeps, more than 9000 partial and complete magnetopause crossings were captured; most with high data rate coverage. During the extended mission, thousands of additional magnetopause crossings have been captured by MMS. The MMS spacecraft have maintained a tight formation during this mission (<60 km separations). For the purposes of this study, observations from a single spacecraft in the constellation is sufficient to represent the entire constellation.

The MMS instrument data sets used in this study are from the Fast Plasma Instrument (FPI) (Pollock et al., 2016) and the Fluxgate Magnetometer (FGM) (Russell et al., 2016; Torbert et al., 2016). The FPI instrument provides rapid ion measurements over the energy range 10 eV/e–30 keV/e, with a temporal resolution of 150 msec (“burst” mode data rate for ions) and 4 s (slower “survey” mode data rate for ions). The FPI ion energy spectrograms and the associated moments are used to identify the regions surrounding the magnetopause (including its boundary layers) and the ion jet reversals associated with magnetopause magnetic reconnection.

The solar wind measurements associated with each of the individual ion jet intervals observed by MMS are from the Wind Solar Wind Experiment (SWE) (Ogilvie et al., 1995) and the Wind Magnetic Field Instrument (MFI) (Lepping et al., 1995). The solar wind convection times to the MMS location at the magnetopause have been estimated by individually lining up magnetic field rotations in the solar wind observed at the Wind satellite with magnetic field rotations in the magnetosheath observed by the MMS/FGM (Trattner et al., 2018). A more detailed description of the methodology for estimating the convection time from the solar wind monitor to the magnetopause is provided in Trattner et al. (2020). These parameters are used for the creation of the dayside magnetopause magnetic shear angle color contour plots and to predict the location of the magnetopause reconnection line using the Maximum Magnetic Shear model (e.g., Trattner et al., 2007). The statistical histograms of IMF orientations during the MMS mission are from the Wind magnetometer, spanning the years 2015–2019 (available at CDAWeb).

## 3. Case Studies

Two cases of ion jet reversals at the magnetopause are presented. The inclusion of these cases is to provide examples of MMS magnetopause crossings in proximity to reconnection sites (based upon ion jet reversals along the  $Z_{\text{GSM}}$  direction) downstream of the quasi-perpendicular and quasi-parallel bow shock, respectively. These cases each occurred during an extended interval of steady solar wind dynamic pressure, when the IMF was close to the nominal Parker-spiral orientation, but with a small southward IMF component. The first described interval was observed by MMS at the low-latitude post-noon magnetopause (downstream of the quasi-perpendicular bow shock region), while the second described interval was observed by MMS at the low-latitude dawn magnetopause (downstream of the quasi-parallel bow shock region).

### Case 1. 17 November 2016

This first case is illustrated in Figure 2, during an outbound pass of the MMS spacecraft. Figure 2a depicts a cartoon of the bow shock and magnetopause (Sun is toward the top of the panel), with an emphasis on the



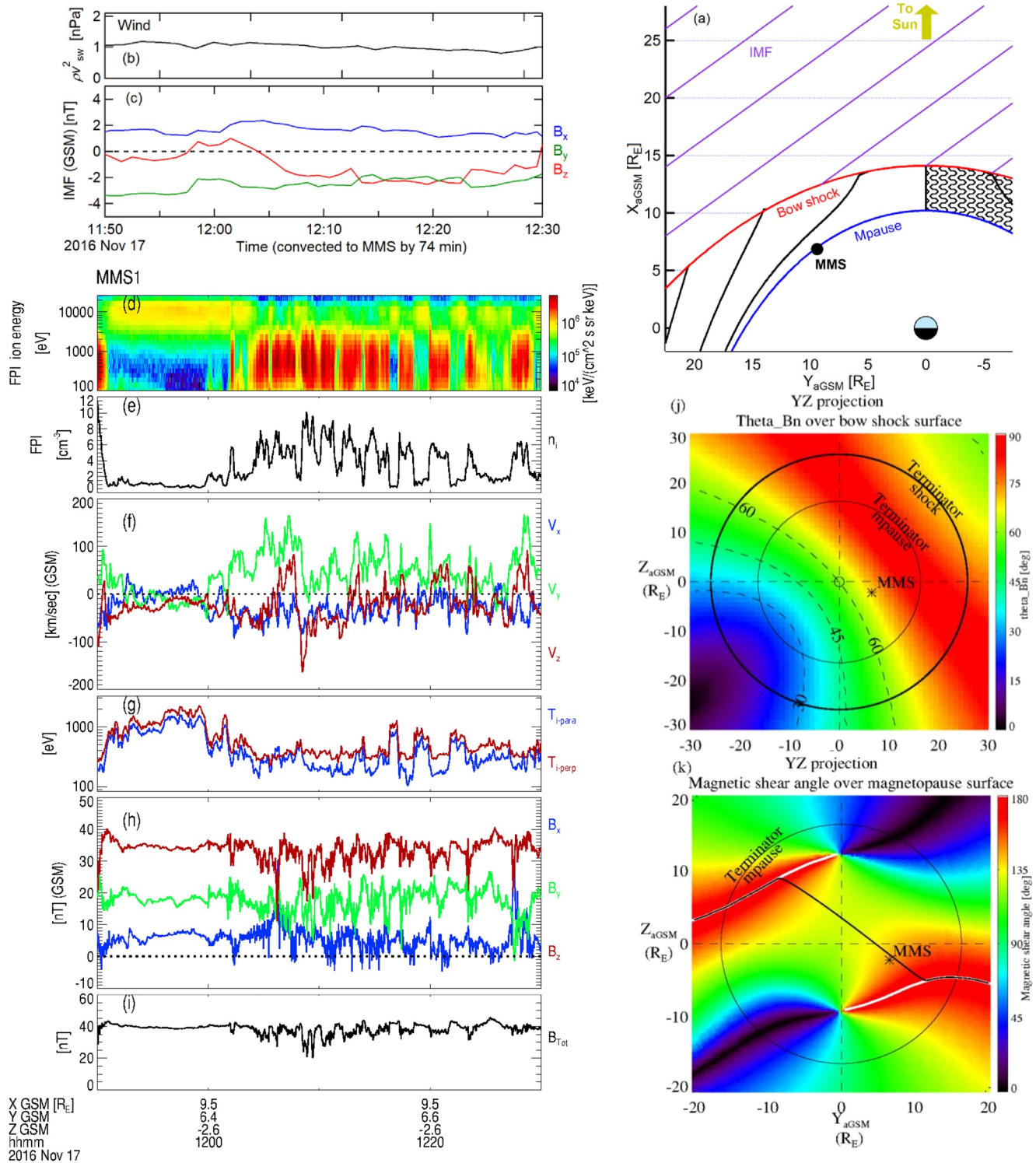


**Figure 2.** Example of ion jet reversals observed by Magnetospheric Multiscale (MMS) at the post-noon magnetopause. (a) Illustration of the interplanetary magnetic field (IMF) (purple lines), streamlines in the magnetosheath (black), and MMS at the magnetopause downstream of the quasi-perpendicular bow shock. (b) Solar wind dynamic pressure. (c) IMF components. (d) MMS ion energy-time spectrogram of energy flux. (e) Ion density. (f) Ion velocity components. (g) Ion temperature parallel and perpendicular to the magnetic field. (h) Magnetic field components. (i) Magnetic field strength. (j) Projected  $\theta_{Bn}$  contour plot at the bow shock surface as viewed from the Sun. (k) Projected magnetic shear angle color contour plot, reconnection line (black trace), and MMS location as viewed from the Sun.

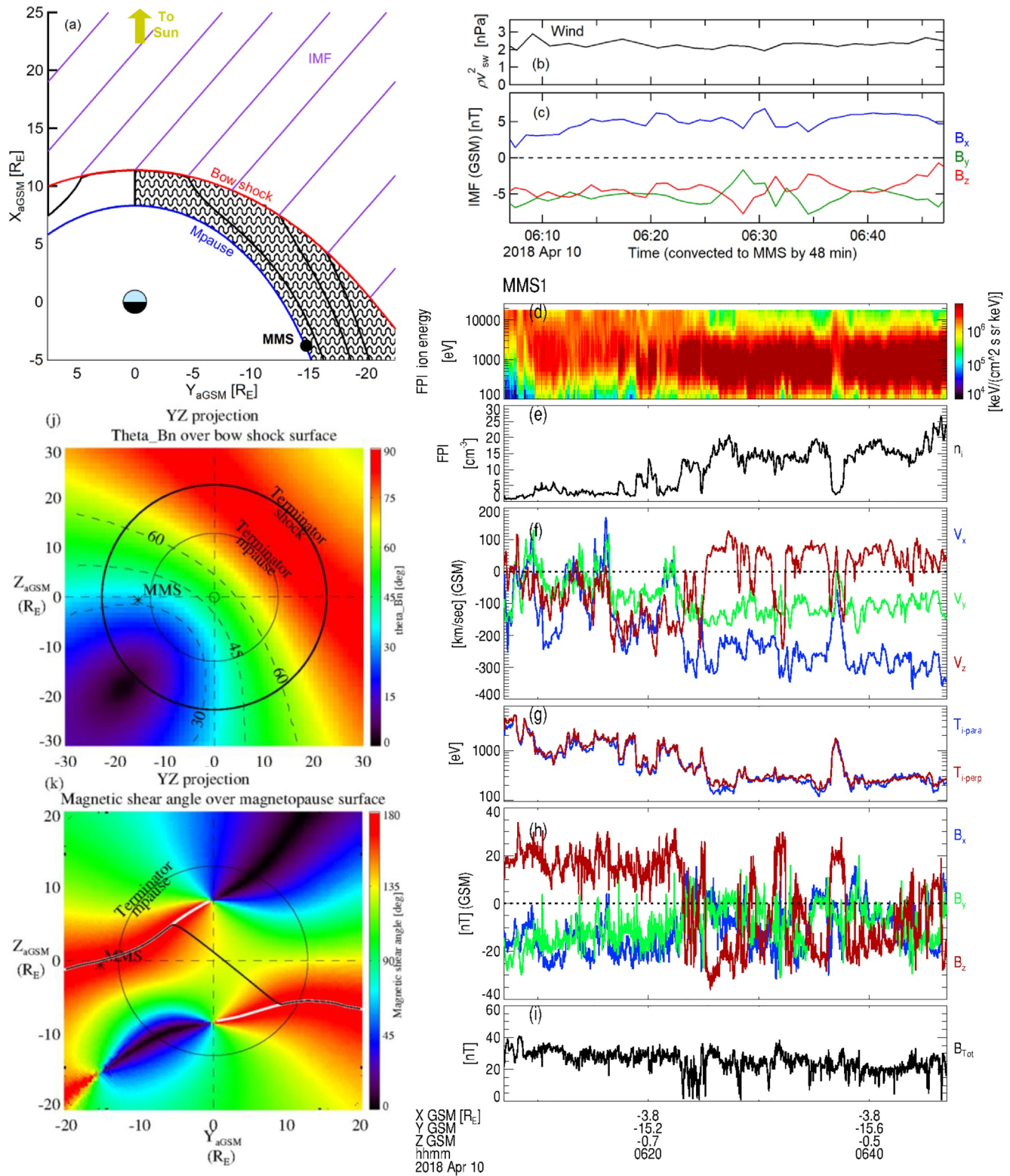
post-noon magnetosheath. The IMF is shown in the upper portion of the panel as purple parallel lines oriented at an angle of  $\sim 55^\circ$  relative to the Sun-Earth line (from panel (c)). Streamlines within the magnetosheath are depicted as black traces between the bow shock and magnetopause. The patterned wave region of the pre-noon/dawnside magnetosheath depicts enhanced variations; similar to that of Figure 1. Figures 2b and 2c show a 40-min interval of the solar wind dynamic pressure and IMF components respectively, as observed by the Wind spacecraft. These traces have been advanced in time by 74 min; the estimated solar wind convection time from Wind in the solar wind to MMS at the magnetopause. Figures 2d–2i show the MMS observations over the same time interval as in panels (b) and (c); 11:50–12:30 UT. Figure 2d shows an energy-time spectrogram of the differential energy flux of ions as measured by FPI. The enhancement of ion flux at  $\sim 10$  keV prior to  $\sim 12:03$  UT, along with the low ion density (Figure 2e) and high ion temperature (Figure 2g) reveals that MMS was within the outer magnetosphere (MMS observed a few nearly complete crossings of the magnetopause a bit prior to ( $\sim 11:25$ – $11:35$  UT) the presented interval). MMS later intermittently sampled the low latitude boundary layer. This is illustrated with significant reductions in the high energy ion population, along with significant enhancements in the ion flux at lower energies (below a few keV). These enhancements in ion energy flux at lower energies were accompanied by significant increases in ion density and reductions in ion temperature. Since the magnetic field components do not show a clear rotation to more closely resemble the IMF (Figure 2h), MMS is surmised to have been close to but not yet crossed the magnetopause current layer. However, the large reversal of the Z-component of the ion bulk velocity at  $\sim 12:07$ – $12:09$  UT, along with subsequent reversals in  $V_z$  (Figure 2f) indicates that MMS was in the vicinity of a reconnection site at the magnetopause (a switch of  $\pm 70$  km/s of the FPI ion velocity moment  $Z_{\text{GSM}}$  component within a 2-min window is designated as a ion jet reversal (Trattner et al., 2017)).

Figure 2j shows the projection of the location of MMS (at the magnetopause) with respect to the bow shock, as viewed along the solar wind flow velocity vector (aberrated GSM coordinates (aGSM)). The color scale represents the angle  $\theta_{\text{Bn}}$  along the Chao et al., 2002 bow shock model surface at 12:08:06 UT; using the measured and convected solar wind plasma moments and IMF orientation. The thick, outer black circle represents the bow shock terminator (slice through the bow shock surface at the  $X_{\text{aGSM}} = 0$  plane), while the thin, inner black circle represents the magnetopause terminator (slice through the magnetopause surface at the  $X_{\text{aGSM}} = 0$  plane). Dashed lines denote  $\theta_{\text{Bn}} = 30^\circ$ ,  $45^\circ$ , and  $60^\circ$ . In this case, MMS was downstream of the quasi-perpendicular bow shock.

Figure 2k shows the projection of the location of MMS with respect to the magnetopause, as viewed along the solar wind flow velocity vector. The color scale in this panel represents the magnetic shear angle across the magnetopause at the time specified above. The thin black circle represents the magnetopause terminator. The black line represents the maximum magnetic shear model (Trattner et al., 2007), where magnetic reconnection is predicted to occur along the dayside magnetopause. The black reconnection line segments along the magnetopause flanks are along the anti-parallel regions (the white line segments represent where the magnetic shear is nearly anti-parallel near local noon), joined along a ridge of maximum magnetic shear at lower latitudes along the dayside magnetopause by a connecting black line segment. The location of MMS was very close to the predicted reconnection line at this time, consistent with the observation of the large reversal in the Z-component of the ion velocity.

#### Case 2. 10 April 2018

This second case is illustrated in Figure 3, during an outbound pass of the MMS spacecraft at the dawn flank. The format of this Figure is similar to that of Figure 2; but with emphasis on the pre-noon/dawnside magnetopause and magnetosheath associated with the region downstream of the quasi-parallel bow shock. Based upon the solar wind observations in Figure 3c, the projected IMF lines shown in Figure 3a are oriented at an angle of  $\sim 40^\circ$  relative to the Sun-Earth line (the solar wind observations have been advanced in time by 48 min; the estimated solar wind convection time from Wind near the L1 Lagrange point to MMS at the magnetopause). Figure 3d shows an energy-time spectrogram of the differential energy flux of ions as measured by FPI. A comparison of the magnetosheath fluxes with that of Figure 2d (plotted on the same scale) shows that the magnetosheath plasma in the region downstream of the quasi-parallel bow shock (Figure 3d) is of significantly higher flux at the higher energies than in the quasi-perpendicular magnetosheath region (Figure 2d). Fluctuations of the magnetic field intensity are also greater in Figure 3i than in Figure 2i, as would be expected for a spacecraft in a region downstream of



**Figure 3.** Example of ion jet reversals observed by Magnetospheric Multiscale (MMS) at the dawn magnetopause. (a) Illustration of the interplanetary magnetic field (IMF) (purple lines), streamlines in the magnetosheath (black), and MMS at the magnetopause downstream of the quasi-parallel bow shock. (b) Solar wind dynamic pressure. (c) IMF components. (d) MMS ion energy-time spectrogram of energy flux. (e) Ion density. (f) Ion velocity components. (g) Ion temperature parallel and perpendicular to the magnetic field. (h) Magnetic field components. (i) Magnetic field strength. (j) Projected  $\theta_{Bn}$  contour plot at the bow shock surface as viewed from the Sun. (k) Projected magnetic shear angle color contour plot, reconnection line, and MMS location as viewed from the Sun.



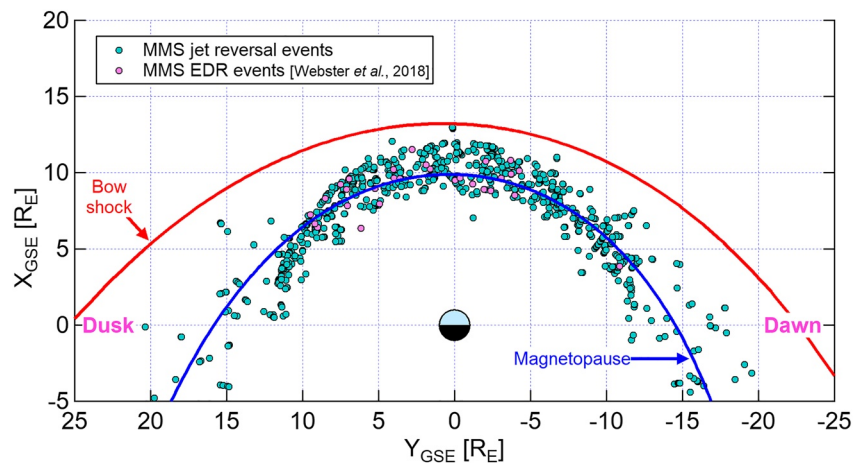


**Figure 4.** The projected locations of the Magnetospheric Multiscale spacecraft during the ion jet reversal and electron diffusion region events, with nominal magnetopause and bow shock boundaries overlaid in blue and red, respectively.

the quasi-parallel bow shock. The enhanced fluctuations just outside the magnetopause are consistent with results of previous studies as described in Section 2.

Several ion jet reversals were observed between 06:24 and 06:31 UT by MMS at the flank magnetopause, as depicted by the Z-component of the bulk ion velocity in Figure 3f. Each ion jet reversal is treated as a distinct and separate event. Figure 3k shows MMS at the anti-parallel leg of the magnetopause flank during this interval, again consistent with the predicted location of magnetic reconnection. Thus, despite MMS sampling the magnetopause in a region downstream of the quasi-parallel bow shock, signatures of magnetic reconnection are observed with ion jet reversals consistent with the spacecraft being in the vicinity of the predicted reconnection line location.

#### 4. Statistical Study of Reconnection at the Magnetopause

An automated routine has been implemented to identify and compile a set of ion jet reversal intervals observed by the MMS spacecraft at the low-latitude dayside magnetopause and within the boundary layers. This technique has been used in previous studies (Petrinec et al., 2016; Trattner et al., 2017; Trattner, Petrinec, & Fuselier, 2021), and is one method by which active magnetopause reconnection is identified with the MMS observations. The reversal in direction (as stated above, determined as a switch of  $\pm 70$  km/s of the MMS/FPI ion velocity moment  $Z_{\text{GSM}}$  component within a 2-min window (Trattner et al., 2017)) indicates that a magnetic reconnection line has passed over the spacecraft (i.e., that the reconnection location is very close to the spacecraft). Such switches can occur either in isolation or in succession. Since these ion jet reversals are observed over a time scale of minutes, these events are described as “steady” reconnection. This is in contrast to more transitory reconnection phenomena such as FTEs. The set of identified intervals has been checked against intervals identified as FTEs (e.g., listing provided by C. Zhao, and utilized in Zhao, 2019). Only  $\sim 10$  intervals were suspect, and were removed from the set of “steady” reconnection intervals. Included within this data set of ion jet reversals is the steady reconnection interval sequence observed by MMS along the dusk flank magnetopause just days prior to the start of the prime mission, as described in detail by Gomez et al., 2016. On occasion, the MMS spacecraft were able to directly sample the EDR of the reconnection site (Burch et al., 2016; Webster et al., 2018), as well as several “near-EDR” encounters (Webster et al., 2018). These intervals (along with convected solar wind parameters, when available) have also been incorporated into this compiled list, resulting in a total of 865 magnetopause encounter intervals wherein MMS was in proximity to the reconnection site; from the start of the mission through December 2019 (four full sweeps of the dayside magnetopause by MMS). As mentioned in the description of Case 2, each  $V_{\text{zGSM}}$  reversal (or EDR encounter) is treated as a distinct and separate event. Multiple encounters at the reconnection site per pass is consistent with enhanced magnetosheath variations causing large-scale motions of the magnetopause as was described in the Russell et al. (1997) study. Figure 4 displays the projected locations of all 865 intervals of ion jet reversals (green) and EDR intervals (fuchsia) into the GSE coordinate equatorial plane, along with a nominal magnetopause (blue) and bow shock (red).

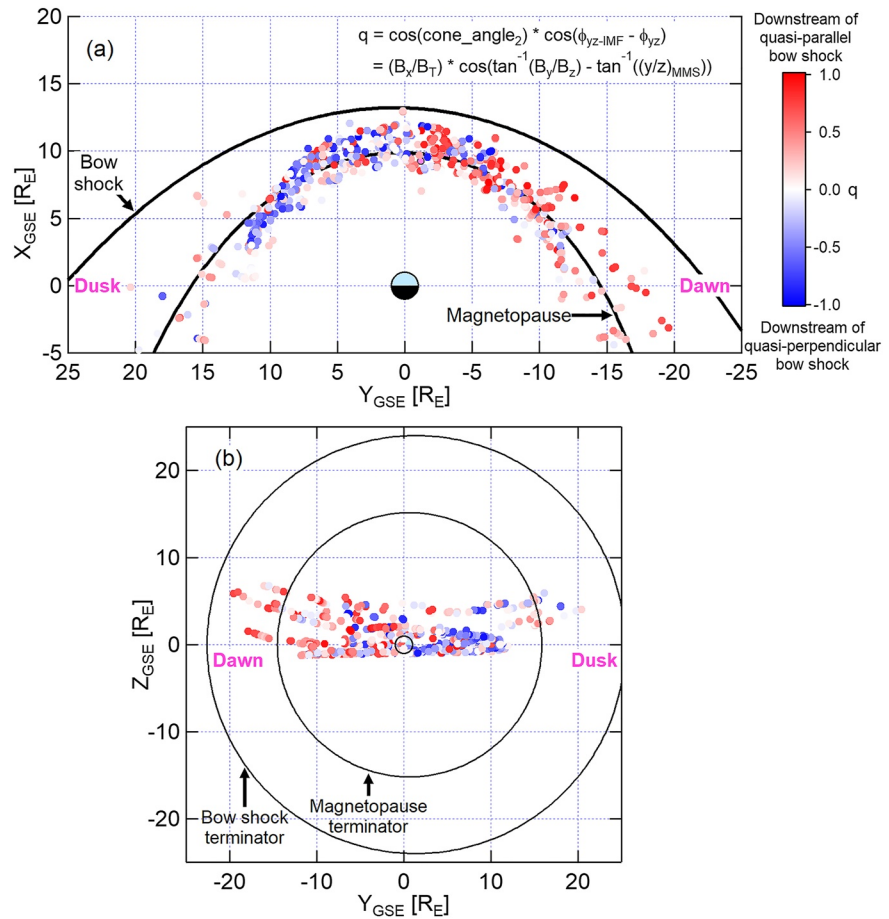


**Figure 5.** The same Magnetospheric Multiscale (MMS) locations as presented in Figure 4, projected into the (a)  $XY_{GSE}$  plane, and (b)  $YZ_{GSE}$  plane. The locations are color-coded by the parameter “ $q$ ”; with positive values (red) indicating when the MMS spacecraft were downstream of the quasi-parallel bow shock ( $q > 0$ ), and negative values (blue) indicating when the MMS spacecraft were downstream of the quasi-perpendicular bow shock ( $q < 0$ ).

Each observed magnetopause reconnection interval is matched with the convected solar wind plasma parameters and IMF, as measured by the Wind spacecraft. Solar wind convection times to the magnetopause have been determined by lining up rotations of the IMF observed at the Wind satellite (Wind/MFI) with magnetic field rotations within the magnetosheath observed by the MMS/FGM (e.g., Trattner et al., 2018; Trattner, Fuselier, et al., 2021). Figure 5a presents the same projected locations of the MMS spacecraft as in Figure 4; but each interval is color-coded by a single parameter “ $q$ ” ( $-1 < q < +1$ ). This parameter captures both the IMF cone\_angle<sub>2</sub> of each interval and the cosine of  $\Delta\phi$  (the YZ-angle of IMF components relative to the YZ-angle of the spacecraft location). Explicitly,  $q = \cos(\text{cone\_angle}_2) * \cos(\phi_{yz-IMF} - \phi_{yz}) = (B_x/B_T) * \cos(\tan^{-1}(B_y/B_z) - \tan^{-1}(y/z)_{MMS})$ . Solid red circles represent locations of MMS when the spacecraft were downstream of the quasi-parallel bow shock ( $q > 0$ ); and solid blue circles represent locations of MMS when the spacecraft were downstream of the quasi-perpendicular bow shock ( $q < 0$ ). Intervals downstream of the quasi-parallel bow shock are preferentially located along the pre-noon/dawnside magnetopause, while intervals downstream of the quasi-perpendicular bow shock are preferentially located along the post-noon/dusk side magnetopause; as expected for an IMF which is commonly oriented along the Parker-spiral direction (cf., Figure 1). Figure 5b shows the projected locations with the same color-coding, as viewed from the Sun toward the Earth.

The statistical analysis of reconnection occurrence begins with an examination of the number of reconnection intervals as observed by MMS as a function of the IMF cone\_angle<sub>2</sub>, and in relation to the general distribution of IMF orientations. The IMF was directed southward ( $B_{z,GSM} < 0$ ) for the majority of these intervals, as expected for the occurrence of magnetic reconnection equatorward of the cusps. It is noted that, especially for a

weak southward IMF component, the draped magnetic field can be locally directed northward (e.g., Šafránková et al., 2009). Nevertheless, anti-parallel magnetic reconnection can still occur along the mid- to high-latitude regions of the dayside and flank magnetopause. Aside from the bias toward southward IMF during these intervals, the existence of other biases of the IMF orientation (e.g., systematic differences between the occurrence of reconnection downstream of the quasi-perpendicular bow shock vs. downstream of the quasi-parallel bow shock) is investigated by constructing histograms of the IMF orientation during this set of MMS intervals, and comparing these histograms with the overall IMF orientation histogram from the 4+ years of solar wind observations. When the IMF has a strong radial component (i.e., dominant IMF  $B_x$ ), the magnetopause everywhere is downstream of the quasi-parallel bow shock. Similarly, when the IMF is predominantly transverse (i.e., small IMF  $B_x$  component), then the magnetopause everywhere is downstream of the quasi-perpendicular bow shock. The intermediate case is when the radial and transverse components of the IMF are of similar magnitudes. In this scenario (as in the case of the nominal Parker spiral angle), one side of the magnetopause lies downstream of the quasi-parallel bow shock, while the opposing side lies downstream of the quasi-perpendicular bow shock (as was shown in Figure 1).

The distribution of IMF orientations during the MMS reconnection intervals is examined in relation to the general IMF distribution for the three separate  $\theta_{Bx2}$  (IMF cone\_angle<sub>2</sub>) regimes: 1) the “radial IMF” regime ( $0^\circ < \text{cone\_angle}_2 < 30^\circ$ , and  $150^\circ < \text{cone\_angle}_2 < 180^\circ$  ( $|B_x|/B_T > 0.87$ ); 2) the “transverse IMF” regime ( $60^\circ < \text{cone\_angle}_2 < 120^\circ$ ); and 3) the “Parker spiral” regime ( $30^\circ < \text{cone\_angle}_2 < 60^\circ$ , and  $120^\circ < \text{cone\_angle}_2 < 150^\circ$ ). While the first two regimes are straightforward for examination, the “Parker spiral” regime requires consideration of the spacecraft location in relation to the IMF orientation. The parameter “ $q$ ” described above is a convenient parameter for this purpose.

The IMF orientations over the entire 4+ years are depicted in Figure 6a as a histogram of IMF cone\_angle<sub>2</sub> (bins of  $3^\circ$  width), using the Wind 5-min resolution data set. Radial IMF conditions occur much less frequently than transverse IMF conditions. There are two peaks in the histogram distribution, corresponding to the Parker spiral angle (at cone\_angle<sub>2</sub> of  $45^\circ$  and  $135^\circ$ ). This histogram can be further separated according to IMF clock angle ( $\tan^{-1}(B_y/B_z)$ ); the negative IMF  $B_y$  component histogram shown is in blue; and positive IMF  $B_y$  component shown in red. Vertical dashed lines demark the three different regimes to be compared with MMS observations.

Figure 6b shows a histogram of the IMF orientations associated with the 865 MMS reconnection intervals overlaid (to scale) upon the general IMF distribution (bins of  $15^\circ$  width). The relative occurrence of reconnection intervals in the radial IMF regime ( $179/865 = 20.7\%$ ) exceeds the general IMF distribution within the same cone\_angle<sub>2</sub> range ( $17.2\%$ ); while the relative occurrence of reconnection intervals in the transverse IMF regime ( $279/865 = 32.3\%$ ) is smaller than the general IMF distribution within the same cone\_angle<sub>2</sub> range ( $41.1\%$ ). The ratio of MMS radial-to-transverse IMF intervals is  $179/279 = 0.64$ , while the same general IMF distribution yields a radial-to-transverse ratio of 0.42. Magnetosheath fluctuations downstream of a quasi-perpendicular bow shock region (i.e., associated with transverse IMF conditions) are significantly smaller in amplitude than those associated with fluctuations downstream of a quasi-parallel bow shock region. In summary, there is a relatively higher than expected probability of observing reconnection sites for a radial IMF configuration (i.e., downstream of a quasi-parallel shock), and there is a relatively lower than expected probability of observing reconnection sites for a transverse IMF configuration (i.e., downstream of a quasi-perpendicular shock). Some probable reasons for the larger than expected occurrence probability of observing reconnection site signatures under radial IMF conditions are: (a) reconnection can potentially occur over much of the dayside magnetopause (as examined with field line models, numerical model runs, and spacecraft observations (e.g., Pi et al., 2017, 2018; Tang et al., 2013)), even if the IMF includes a very small northward component, and (b) small changes in the radial IMF orientation can cause large changes in the location of magnetic reconnection along the dayside magnetopause.

In order to further examine the effect of IMF orientation on the occurrence probability of observing signatures at a reconnection site, the Parker spiral angle and ortho Parker spiral angle categories are compared. The remainder of the MMS reconnection intervals (407 of 865) occur for IMF conditions within  $15^\circ$  of the Parker spiral angle (304 of 407 intervals), or the ortho Parker spiral angle (103 of 407 intervals). These are the conditions for which a spatial (e.g., dawn-dusk) asymmetry exists in magnetosheath fluctuations (as in Figure 1); and may manifest in the probability of reconnection site encounters, depending on whether the sampling spacecraft is downstream of the quasi-parallel or quasi-perpendicular bow shock region. Considering both the IMF clock and cone\_angle<sub>2</sub> values, and considering whether MMS was in the pre-noon/dawnside or post-noon/duskside sector,

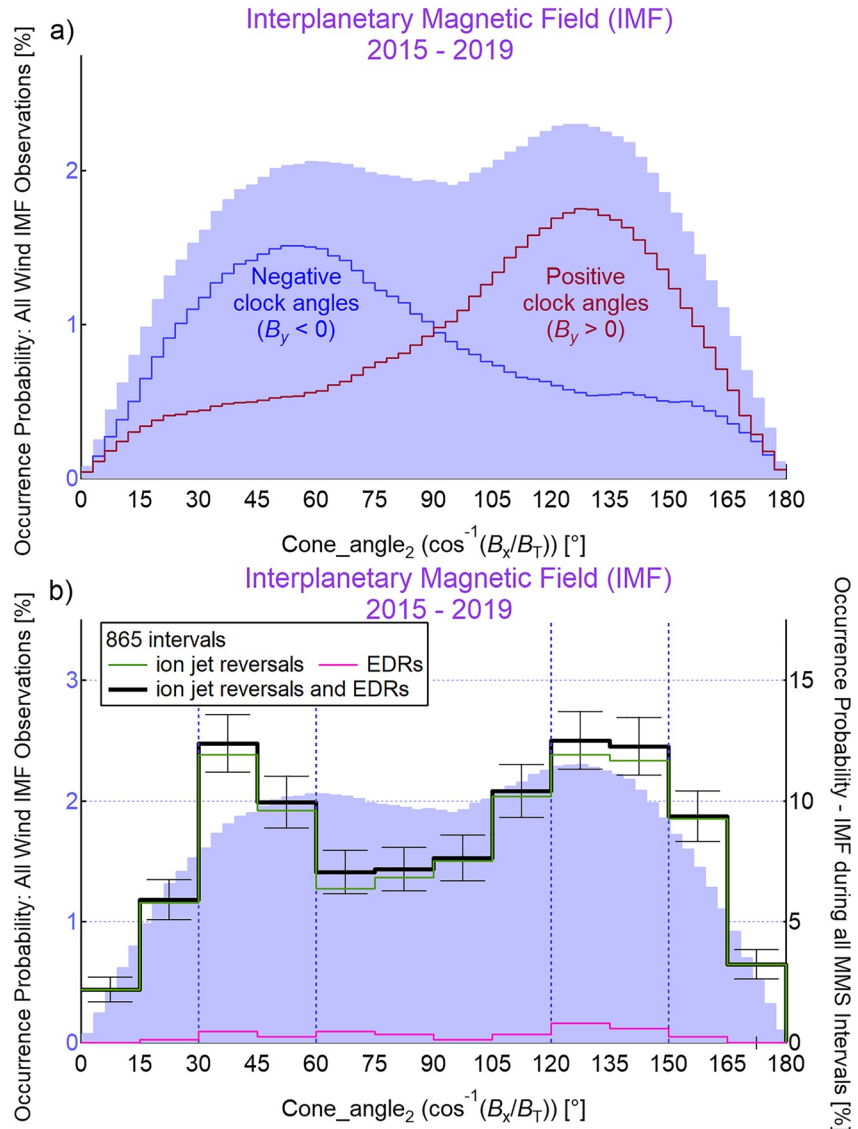


**Figure 6.** (a) Occurrence probability histogram of all observed interplanetary magnetic field (IMF) orientations spanning the times of the Magnetospheric Multiscale (MMS) magnetopause reconnection intervals, as a function of cone\_angle<sub>2</sub>. The overall histogram is separated into two histograms according to the sign of the IMF clock angle (blue: negative; red: positive). (b) Same as panel (a), but with the occurrence probability histogram of the IMF cone\_angle<sub>2</sub> values associated with the ion jet reversals and electron diffusion regions as observed by MMS. Histogram error bars reflect Poisson statistical uncertainty ( $N^{1/2}$ ) prior to normalization.

225 magnetopause reconnection intervals were found to be downstream of the quasi-parallel bow shock, while 182 intervals were downstream of the quasi-perpendicular bow shock. Again, signatures of magnetic reconnection in proximity to MMS occurred more often in the region downstream of the quasi-parallel bow shock than in the region downstream of the quasi-perpendicular bow shock.

These results are consistent with those of Russell et al. (1997), using ISEE observations of the number of magnetopause crossings and associated oscillation amplitude. That is, a statistically larger number of magnetopause oscillations were observed at the pre-noon magnetopause than at the post-noon magnetopause. Figure 4 illustrates this result, with a somewhat greater number of events located near dawn than near dusk (the average aberration angle of the solar wind flow may also contribute to the flank asymmetry via orbital bias). However, this does not mean that magnetic reconnection is enhanced at the magnetopause downstream of the quasi-parallel bow shock relative to the magnetopause downstream of the quasi-perpendicular bow shock. Rather, this result merely



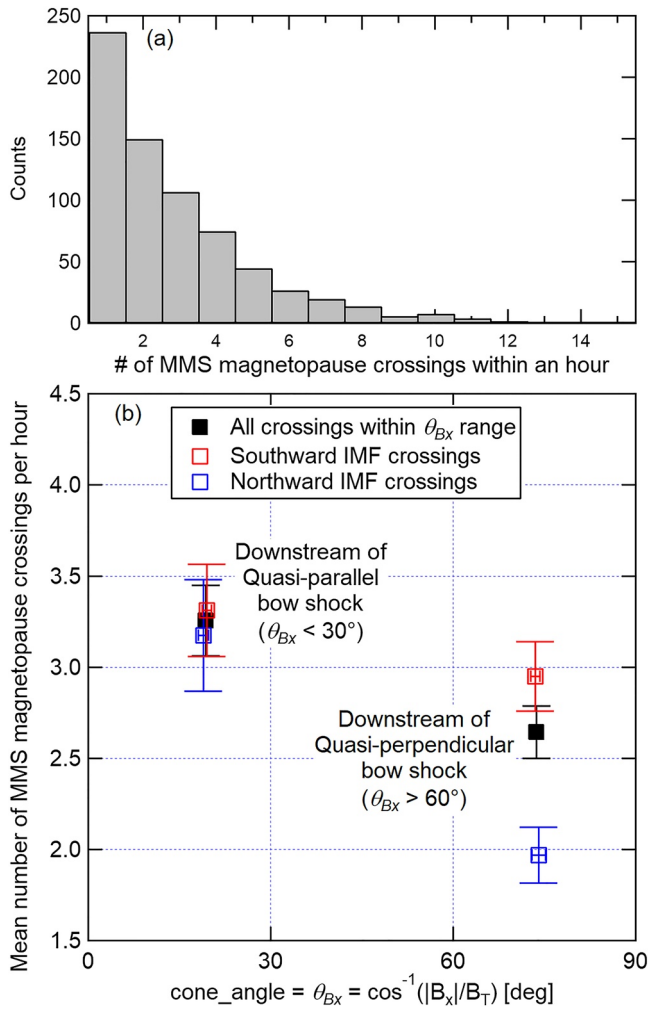


**Figure 7.** (a) Histogram of the number of magnetopause crossings per hour, as observed by Magnetospheric Multiscale. (b) Mean number of magnetopause crossings per hour, during conditions of “radial interplanetary magnetic field (IMF)” ( $\theta_{Bx} < 30^\circ$ ) and during conditions of “transverse IMF” ( $\theta_{Bx} > 60^\circ$ ). Partitioning by IMF  $B_{zGSM}$ , the mean number of magnetopause crossings per hour is greater when the IMF is southward than when it is northward.

supports the results of the earlier ISEE study that magnetopause oscillations are enhanced in the region associated with the quasi-parallel bow shock.

As an independent check of the assertion that there is greater large-scale motion of the magnetopause downstream of the quasi-parallel bow shock, the number of magnetopause crossings per hour as observed by MMS during the prime mission and as a function of  $\theta_{Bx}$  is examined here ( $\theta_{Bx} = \cos^{-1}(|B_x|/B_T)$ ). The MMS magnetopause crossing data set used is that which was carefully constructed and investigated by Haaland et al. (2020). A histogram of the number of magnetopause crossings per hour is presented in Figure 7a. While many isolated magnetopause crossings (i.e., one crossing per hour) were observed, the majority of the time multiple magnetopause crossings occurred within an hour; with as many as 15 distinct magnetopause crossings observed by MMS within a single hour. In Figure 7b, the mean number of magnetopause crossings per hour has been determined from this MMS magnetopause crossing set; when the dayside magnetopause was downstream of the quasi-parallel bow shock (“radial IMF”:  $\theta_{Bx} < 30^\circ$ ), and when the dayside magnetopause was downstream of the quasi-perpendicular bow shock (“transverse IMF”:  $60^\circ < \theta_{Bx} < 90^\circ$ ). Consistent with the results of Russell et al. (1997), the average number of magnetopause crossings per hour is greater when MMS was downstream of the quasi-parallel bow shock than when MMS was downstream of the quasi-perpendicular bow shock. Separating each category by the z-component of the IMF, the average number of magnetopause crossings per hour is greater during intervals of southward IMF than during northward IMF; again consistent with the ISEE results presented by Russell et al. (1997).

To further investigate whether magnetic reconnection is enhanced (or inhibited) at the magnetopause downstream of the quasi-parallel bow shock, the distances of the MMS ion jet reversals and EDR encounters (all of which are in proximity to the reconnection site) from the predicted locations of magnetic reconnection are examined in a statistical manner. These distances are the minimum 3D path lengths from the spacecraft along the magnetopause surface to the model reconnection line. If the distribution of actual distances of the sampling spacecraft from the locations of the model reconnection lines is relatively large, then enhanced magnetosheath fluctuations could be implicated in initiating reconnection at random locations at the magnetopause; rather than at the preferred (i.e., predicted) reconnection line location. Of the 865 intervals of this data set, 461 intervals are designated as being downstream of the quasi-perpendicular bow shock (i.e., “ $q$ ” < 0). The distribution of 3D path lengths of MMS from the predicted reconnection line

of each interval is displayed in Figure 8a. The mode of the distribution is at  $\sim 1.0$ – $1.5 R_E$  from the model reconnection line. The spacecraft was sometimes at a significantly greater distance from the model reconnection line, resulting in a Poisson-like distribution with a median distance of  $2.6 R_E$  and a mean value of  $3.1 R_E$ . To determine the uncertainties of the histogram bins, the inherent uncertainty of the reconnection line model is  $\sim 1 R_E$  for nominal conditions (IMF  $|B_x|/B_T < 0.8$ , or cone\_angle >  $36.87^\circ$ ), as described in earlier studies (Trattner et al., 2007; Trattner, Petrinc, & Fuselier, 2021). For this subset of 461 intervals, an uncertainty of  $-1 R_E < \Delta r < +1 R_E$  is added to the 3D distance (path length) of each interval (using a uniform random number generator), and a distance histogram is determined. This process is repeated 1000 times (resulting in 1000 distance histograms), and the SD of the number of samples of each histogram bin is calculated. This is represented by the error bars in Figure 8a.

Figure 8b shows a distribution of distances for the 404 intervals during which MMS was designated as being downstream of the quasi-parallel bow shock (i.e., “ $q$ ” > 0). As in Figure 8a, the mode of the distance distribution is at  $\sim 1.0$ – $1.5 R_E$  from the model reconnection line, with a median distance of  $2.3 R_E$  and a mean value of  $3.4 R_E$ . The procedure to estimate the uncertainties associated with each histogram bin is similar to that described

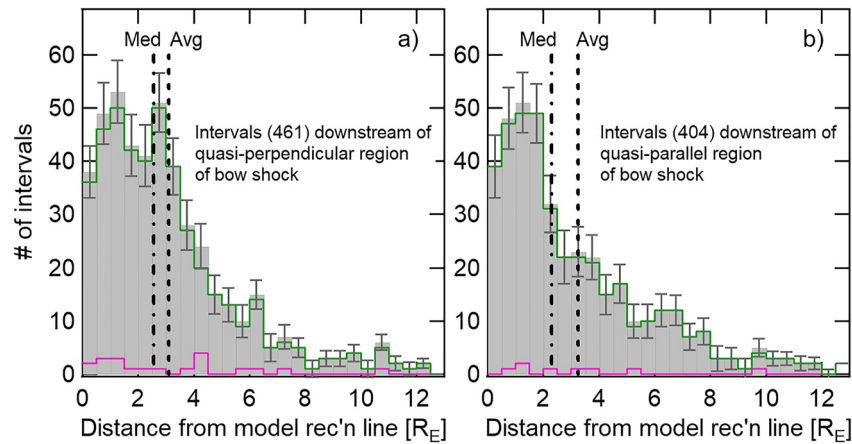


**Figure 8.** Histograms of the 3D distances of ion jet reversals (green) and electron diffusion regions (fuchsia) and summed histograms (gray) from the predicted reconnection site. (a) Events downstream of the quasi-perpendicular bow shock. (b) Events downstream of the quasi-parallel bow shock.

above, However, it is realized that the inherent error of the models used to produce the predicted reconnection line location becomes larger for a largely radial IMF condition. Therefore, the uncertainty added to interval is  $\sim 1 R_E$  for those occurring under nominal conditions ( $IMF |B_x|/B_T < 0.8$ , or  $\text{cone\_angle} > 36.87^\circ$ ),  $\sim 2 R_E$  for those occurring under more radial conditions ( $0.8 < IMF |B_x|/B_T < 0.95$ , or  $18.19^\circ < \text{cone\_angle} < 36.87^\circ$ ), and  $\sim 3 R_E$  for those occurring under strongly radial conditions ( $IMF |B_x|/B_T > 0.95$ , or  $\text{cone\_angle} < 18.19^\circ$ ). Using the procedure described above, 1000 distance histograms are constructed using randomized added uncertainties for each interval, and the SD of the number of samples of each histogram bin is calculated. This is represented by the error bars in Figure 8b.

The conclusion of this comparison of distance histograms for intervals downstream of the quasi-parallel bow shock and those intervals downstream of the quasi-perpendicular bow shock is that there is no systematic statistical difference of the distances of observed reconnection intervals from the predicted locations of reconnection lines.

## 5. Summary

A statistical investigation has been conducted of the IMF orientation in relation to MMS magnetopause intervals for which reconnection signatures were observed (ion jet reversals and EDR encounters). The first part of this study investigated the occurrence of these magnetopause intervals downstream of either the quasi-parallel or quasi-perpendicular bow shock, in comparison to the general distribution of IMF orientations. While there was a statistically significant enhancement in the number of intervals observed downstream of the quasi-parallel bow shock in comparison to the number downstream of the quasi-perpendicular bow shock, it has not been determined that this is a result of enhanced reconnection caused by increased magnetosheath fluctuations (as has been suggested by the results of a recent hybrid simulation under nearly radial IMF with a small northward component (Chen et al., 2021)). Rather, the increased magnetosheath fluctuations downstream of the quasi-parallel bow shock are believed to cause large scale oscillations of the magnetopause surface. This result is in accordance with the earlier statistical study by Russell et al., 1997. The propagation of foreshock compressional waves as pressure pulses and the resultant enhancement of magnetopause surface perturbations for the condition of purely radial IMF has also been observed in a three-dimensional global-scale hybrid model simulation (Lin & Wang, 2005). A multi-point case study of a significant yet localized large-scale motion of the subsolar magnetopause surface occurring during radial IMF as observed in situ by the THEMIS spacecraft was described in detail by Shue et al., 2009. Other described processes that contribute to enhanced magnetopause motions are magnetosheath pressure pulses caused by region transitions between a quasi-perpendicular and a quasi-parallel bow shock - especially as a result of a solar wind discontinuity (Archer et al., 2012), and magnetosheath high-speed jets that impact the magnetopause (Plaschke et al., 2018).

The Kelvin-Helmholtz (KH) instability can also produce oscillatory behavior of the flank magnetopause surface. The instability starts as a boundary wave, growing and evolving into vortical structures as the instability is convected far downstream (Hasegawa et al., 2006; Takagi et al., 2006). It is noted that the KH instability occurs much more often for northward than for southward IMF (Kavosi & Raeder, 2015), though there have been occasional observational case studies of KH under radial IMF conditions (Farrugia et al., 2014; Grygorov et al., 2016), or during southward IMF (Hwang et al., 2011). This is in contrast to the intervals of reconnection signatures in this study, the majority of which occurred during southward IMF.

The second part of this study investigated the locations of reconnection signatures in relation to the predicted steady reconnection lines. An examination of histograms of the 3D path lengths of observed reconnection site locations (i.e., local reconnection signatures) in relation to the maximum magnetic shear model predictions reveals no statistically significant differences between intervals observed downstream of the quasi-parallel bow shock and those observed downstream of the quasi-perpendicular bow shock. This result suggests that increased magnetosheath fluctuations are unlikely to initiate magnetic reconnection at random magnetopause locations, and implies that increased fluctuations do not enhance magnetic reconnection at the magnetopause.

## Data Availability Statement

These instrument data sets are available at CDAWeb ([http://cdaweb.gsfc.nasa.gov/istp\\_public/](http://cdaweb.gsfc.nasa.gov/istp_public/)). All Magnetospheric Multiscale (MMS) observations presented within this study are available to the general public via the MMS website (<https://lasp.colorado.edu/mms/sdc/public/about/>).

## Acknowledgments

The Wind Solar Wind Experiment (Wind/SWE) (Ogilvie et al., 1995) and Magnetic Field Instrument (Wind/MFI) (Lepping et al., 1995) provided the solar wind plasma moment and interplanetary magnetic field observations, respectively. The Geotail Magnetic Field Experiment provided the magnetosheath magnetic field observations. Research at Lockheed Martin was performed on Contracts 499935Q and 80NSSC18K1379. Research at LASP is supported by NASA grant NNX14AF71G and 80NSSC20K0688. Research at SWRI was funded by NASA grant NNX11AF71G.

## References

- Anderson, R. R., Harvey, C. C., Hoppe, M. M., Tsurutani, B. T., Eastman, T. E., & Etcheto, J. (1982). Plasma waves near the magnetopause. *Journal of Geophysical Research*, 87(A4), 2087–2107. <https://doi.org/10.1029/ja087ia04p02087>
- Archer, M. O., Horbury, T. S., & Eastwood, J. P. (2012). Magnetosheath pressure pulses: Generation downstream of the bow shock from solar wind discontinuities. *Journal of Geophysical Research*, 117(A5), A05228. <https://doi.org/10.1029/2011JA017468>
- Aubry, M. P., Russell, C. T., & Kivelson, M. G. (1970). Inward motion of the magnetopause before a substorm. *Journal of Geophysical Research*, 75(34), 7018–7030. <https://doi.org/10.1029/ja075i034p07018>
- Bobra, M. G., Petrinec, S. M., Fuselier, S. A., Claffin, E. S., & Spence, H. E. (2004). On the solar wind control of cusp aurora during northward IMF. *Geophysical Research Letters*, 31(4), L04805. <https://doi.org/10.1029/2003GL018417>
- Burch, J. L., Torbert, R. B., Phan, T. D., Chen, L. J., Moore, T. E., Ergun, R. E., et al. (2016). Electron-scale measurements of magnetic reconnection in space. *Science*, 352(6290), aaf2939. <https://doi.org/10.1126/science.aaf2939>
- Chao, J. K., Wu, D. J., Lin, C.-H., Yang, Y. H., Wang, X. Y., Kessel, M., et al. (2002). Models for the size and shape of the Earth's magnetopause and bow shock. In L.-H. Lyu (Ed.), *Space weather study using multipoint techniques, COSPAR Colloq. Ser.* (Vol. 12, pp. 127–134). Pergamon. [https://doi.org/10.1016/S0964-2749\(02\)80212-8](https://doi.org/10.1016/S0964-2749(02)80212-8)
- Chen, L.-J., Ng, J., Omelchenko, Y., & Wang, S. (2021). Magnetopause reconnection and indentations induced by foreshock turbulence. *Geophysical Research Letters*, 48(11), e2021GL093029. <https://doi.org/10.1029/2021GL093029>
- Cowley, S. W. H., & Owen, C. J. (1989). A simple illustrative model of open flux tube motion over the dayside magnetopause. *Planetary and Space Science*, 37(11), 1461–1475. [https://doi.org/10.1016/0032-0633\(89\)90116-5](https://doi.org/10.1016/0032-0633(89)90116-5)
- Crooker, N. U. (1979). Dayside merging and cusp geometry. *Journal of Geophysical Research*, 84(A3), 951–959. <https://doi.org/10.1029/ja084ia03p00951>
- Denton, R. E., Gary, S. P., Li, X., Anderson, B. J., LaBelle, J. W., & Lessard, M. (1995). Low-frequency fluctuations in the magnetosheath near the magnetopause. *Journal of Geophysical Research*, 100(A4), 5665–5679. <https://doi.org/10.1029/94ja03024>
- Desroche, M., Bagenal, F., Delamere, P. A., & Erkaev, N. (2012). Conditions at the expanded Jovian magnetopause and implications for the solar wind interaction. *Journal of Geophysical Research*, 117(A7), A07202. <https://doi.org/10.1029/2012JA017621>
- Desroche, M., Bagenal, F., Delamere, P. A., & Erkaev, N. (2013). Conditions at the magnetopause of Saturn and implications for the solar wind interaction. *Journal of Geophysical Research: Space Physics*, 118(6), 3087–3095. <https://doi.org/10.1002/jgra.50294>
- Dimmock, A. P., Nykyri, K., & Pulkkinen, T. I. (2014). A statistical study of magnetic field fluctuations in the dayside magnetosheath and their dependence on upstream solar wind conditions. *Journal of Geophysical Research: Space Physics*, 119(8), 6231–6248. <https://doi.org/10.1002/2014JA020009>
- Doss, C., Komar, C., Cassak, P., Wilder, F., Eriksson, S., & Drake, J. (2015). Asymmetric magnetic reconnection with a flow shear and applications to the magnetopause. *Journal of Geophysical Research: Space Physics*, 120(9), 7748–7763. <https://doi.org/10.1002/2015JA021489>
- Dunlop, M. W., Zhang, Q.-H., Bogdanova, Y. V., Trattner, K. J., Pu, Z., Hasegawa, H., et al. (2011). Magnetopause reconnection across wide local time. *Annales de Geophysique*, 29(9), 1683–1697. <https://doi.org/10.5194/angeo-29-1683-2011>
- Escoubert, C. P., Smith, M. F., Fung, S. F., Anderson, P. C., Hoffman, R. A., Basinska, E. M., & Bosqued, J. M. (1992). Staircase ion signature in the polar cusp: A case study. *Geophysical Research Letters*, 19(17), 1735–1738. <https://doi.org/10.1029/92gl01806>
- Fairfield, D. H., & Ness, N. F. (1970). Magnetic field fluctuations in the Earth's magnetosheath. *Journal of Geophysical Research*, 75(31), 6050–6060. <https://doi.org/10.1029/ja075i031p06050>
- Farrugia, C. J., Gratton, F. T., Gnani, G., Torbert, R. B., & Wilson, L. B., III. (2014). A vortical dawn flank boundary layer for near-radial IMF: Wind observations on 24 October 2001. *Journal of Geophysical Research: Space Physics*, 119(6), 4572–4590. <https://doi.org/10.1002/2013JA019578>
- Frey, H. U., Mende, S. B., Immel, T. J., Fuselier, S. A., Claffin, E. S., Gerard, J.-C., & Hubert, B. (2002). Proton aurora in the cusp. *Journal of Geophysical Research*, 107(A7), 1091. <https://doi.org/10.1029/2001JA900161>

- Frey, H. U., Phan, T. D., Fuselier, S. A., & Mende, S. B. (2003). Continuous magnetic reconnection at Earth's magnetopause. *Nature*, 426(6966), 533–537. <https://doi.org/10.1038/nature02084>
- Fuselier, S. A., Frahm, R., Lewis, W. S., Masters, A., Mukherjee, J., Petrinec, S. M., & Sillanpaa, I. J. (2014). The location of magnetic reconnection at Saturn's magnetopause: A comparison with Earth. *Journal of Geophysical Research: Space Physics*, 119(4), 2563–2578. <https://doi.org/10.1002/2013JA019684>
- Fuselier, S. A., Frey, H. U., Trattner, K. J., Mende, S. B., & Burch, J. L. (2002). Cusp aurora dependence on interplanetary magnetic field  $B_z$ . *Journal of Geophysical Research*, 107(A7), 1111. <https://doi.org/10.1029/2001JA900165>
- Fuselier, S. A., Petrinec, S. M., Sawyer, R. P., Mukherjee, J., & Masters, A. (2020). Suppression of magnetic reconnection at Saturn's low-latitude magnetopause. *Journal of Geophysical Research: Space Physics*, 125(5), e2020JA027895. <https://doi.org/10.1029/2020JA027895>
- Gomez, R. G., Vines, S. K., Fuselier, S. A., Cassak, P. A., Strangeway, R. J., Petrinec, S. M., et al. (2016). Stable reconnection at the dusk flank magnetopause. *Geophysical Research Letters*, 43(18), 9374–9382. <https://doi.org/10.1002/2016GL069692>
- Gonzalez, W. D., & Mozer, F. S. (1974). A quantitative model for the potential resulting from reconnection with an arbitrary interplanetary magnetic field. *Journal of Geophysical Research*, 79(28), 4186–4194. <https://doi.org/10.1029/ja079i028p04186>
- Gosling, J. T., Asbridge, J. R., Bame, S. J., Feldman, W. C., Paschmann, G., Scokpe, N., & Russell, C. T. (1982). Evidence for quasi-stationary reconnection at the dayside magnetopause. *Journal of Geophysical Research*, 87(A4), 2147. <https://doi.org/10.1029/ja087ia04p02147>
- Gosling, J. T., Thomsen, M. F., Bame, S. J., Elphic, R. C., & Russell, C. T. (1990a). Cold ion beams in the low latitude boundary layer during accelerated flow events. *Geophysical Research Letters*, 17(12), 2245–2248. <https://doi.org/10.1029/GL017i012p02245>
- Gosling, J. T., Thomsen, M. F., Bame, S. J., Elphic, R. C., & Russell, C. T. (1990b). Plasma flow reversals at the dayside magnetopause and the origin of asymmetric polar cap convection. *Journal of Geophysical Research*, 95(A6), 8073–8084. <https://doi.org/10.1029/JA095iA06p08073>
- Gosling, J. T., Thomsen, M. F., Bame, S. J., & Russell, C. T. (1986). Accelerated plasma flows at the near-tail magnetopause. *Journal of Geophysical Research*, 91(A3), 3029–3041. <https://doi.org/10.1029/JA091iA03p03029>
- Grygorov, K., Němeček, Z., Šafránková, J., Prech, L., Pi, G., & Shue, J.-H. (2016). Kelvin-Helmholtz wave at the subsolar magnetopause boundary layer under radial IMF. *Journal of Geophysical Research: Space Physics*, 121(10), 9863–9879. <https://doi.org/10.1002/2016JA023068>
- Gutynska, O., Šimůnek, J., Šafránková, J., Němeček, Z., & Prech, L. (2012). Multipoint study of magnetosheath magnetic field fluctuations and their relation to the foreshock. *Journal of Geophysical Research*, 117(A4), A04214. <https://doi.org/10.1029/2011JA017240>
- Haaland, S., Paschmann, G., Øieroset, M., Phan, T., Hasegawa, H., Fuselier, S., et al. (2020). Characteristics of the flank magnetopause: MMS results. *Journal of Geophysical Research*, 125(3), e2019JA027623. <https://doi.org/10.1029/2019JA027623>
- Hasegawa, H., Fujimoto, M., Takagi, K., Saito, Y., Mukai, T., & Rème, H. (2006). Single-spacecraft detection of rolled-up Kelvin-Helmholtz vortices at the flank magnetopause. *Journal of Geophysical Research*, 111(A9), A09203. <https://doi.org/10.1029/2006JA011728>
- Hietala, H., Phan, T. D., Angelopoulos, V., Øieroset, M., Archer, M. O., Karlsson, T., & Plaschke, F. (2018). In situ observations of a magnetosheath high-speed jet triggering magnetopause reconnection. *Geophysical Research Letters*, 45(4), 1732–1740. <https://doi.org/10.1002/2017GL076525>
- Hwang, K.-J., Kuznetsova, M. M., Sahraoui, F., Goldstein, M. L., Lee, E., & Parks, G. K. (2011). Kelvin-Helmholtz waves under southward interplanetary magnetic field. *Journal of Geophysical Research*, 116(A8), A08210. <https://doi.org/10.1029/2011JA016596>
- Kavosi, S., & Raeder, J. (2015). Ubiquity of Kelvin-Helmholtz waves at Earth's magnetopause. *Nature Communications*, 6(1), 7019. <https://doi.org/10.1038/ncomms8019>
- Kawano, H., & Russell, C. T. (1996). Survey of flux transfer events observed with the ISEE-1 spacecraft: Rotational polarity and the source region. *Journal of Geophysical Research*, 101(27), 27299–27308. <https://doi.org/10.1029/96ja02703>
- Lavraud, B., Fedorov, A., Budnik, E., Thomsen, M. F., Grigoriev, A., Cargill, P. J., et al. (2005). High-altitude cusp flow dependence on IMF orientation: A 3-year cluster statistical study. *Journal of Geophysical Research*, 110(A2), A02209. <https://doi.org/10.1029/2004JA010804>
- Lepping, R. P., Acuna, M. H., Burlaga, L. F., Farrell, W. M., Slavin, J. A., Schatten, K. H., et al. (1995). The WIND magnetic field investigation. *Space Science Reviews*, 71(1–4), 207–229. <https://doi.org/10.1007/BF00751330>
- Li, H., Jiang, W., Wang, C., Verscharen, D., Zeng, C., Russell, C. T., et al. (2020). Evolution of the Earth's magnetosheath turbulence: A statistical study based on MMS observations. *ApJL*, 898(2), L43. <https://doi.org/10.3847/2041-8213/aba531>
- Lin, Y., & Wang, X. (2005). Three-dimensional global hybrid simulation of dayside dynamics associated with the quasi-parallel bow shock. *Journal of Geophysical Research*, 110(A12), A12216. <https://doi.org/10.1029/2005JA011243>
- Luhmann, J. G., Russell, C. T., & Elphic, R. C. (1986). Spatial distributions of magnetic field fluctuations in the dayside magnetosheath. *Journal of Geophysical Research*, 91(A2), 1711–1715. <https://doi.org/10.1029/ja091ia02p01711>
- Luhmann, J. G., Walker, R. J., Russell, C. T., Crooker, N. U., Spreiter, J. R., & Stahara, S. S. (1984). Patterns of potential magnetic field merging sites on the dayside magnetopause. *Journal of Geophysical Research*, 89(A3), 1739–1742. <https://doi.org/10.1029/ja089ia03p01739>
- Masters, A., Eastwood, J. P., Swisdak, M., Thomsen, M. F., Russell, C. T., Sergis, N., et al. (2012). The importance of plasma  $\beta$  conditions for magnetic reconnection at Saturn's magnetopause. *Geophysical Research Letters*, 39(8), L08130. <https://doi.org/10.1029/2012GL051372>
- Němeček, Z., Šafránková, J., Prech, L., Zastenker, G. N., Eiges, P., Nozrachev, M. N., et al. (2000). Magnetosheath study: Interball observations. *Advances in Space Research*, 25(7–8), 1511–1516. [https://doi.org/10.1016/s0273-1177\(99\)00663-8](https://doi.org/10.1016/s0273-1177(99)00663-8)
- Newell, P. T., & Meng, C.-I. (1991). Ion acceleration at the equatorward edge of the cusp: Low-altitude observations of patchy merging. *Geophysical Research Letters*, 18(10), 1829–1832. <https://doi.org/10.1029/91gl02088>
- Ogilvie, K. W., Chornay, D. J., Fritzenreiter, R. J., Hunsaker, F., Keller, J., Lobell, J., et al. (1995). SWE, a comprehensive plasma instrument for the WIND spacecraft. *Space Science Reviews*, 71(1–4), 55–77. <https://doi.org/10.1007/BF00751326>
- Paschmann, G., Fuselier, S. A., & Klumpp, D. M. (1989). High speed flows of  $H^+$  and  $He^{++}$  ions at the magnetopause. *Geophysical Research Letters*, 16(6), 567–570. <https://doi.org/10.1029/gl016i006p00567>
- Petrinec, S. M. (2013). On the magnetic field configuration of the magnetosheath. *Terrestrial, Atmospheric and Oceanic Sciences*, 24(2), 265–272. <https://doi.org/10.3319/TAO.2012.10.17.02>
- Petrinec, S. M., Burch, J. L., Fuselier, S. A., Gomez, R. G., Lewis, W., Trattner, K. J., et al. (2016). Comparison of Magnetospheric Multiscale ion jet signatures with predicted reconnection site locations at the magnetopause. *Geophysical Research Letters*, 43(12), 5997–6004. <https://doi.org/10.1002/2016GL069626>
- Petrinec, S. M., Trattner, K. J., & Fuselier, S. A. (2003). Steady reconnection during intervals of northward IMF: Implications for magnetosheath properties. *Journal of Geophysical Research*, 108(A12), 1458. <https://doi.org/10.1029/2003JA009979>
- Phan, T. D., Frey, H. U., Frey, S., Peticolas, L., Fuselier, S., Carlson, C., et al. (2003). Simultaneous Cluster and IMAGE observations of cusp reconnection and auroral spot for northward IMF. *Geophysical Research Letters*, 30(10), 1509. <https://doi.org/10.1029/2003GL018885>
- Phan, T. D., Kistler, L. M., Klecker, B., Haerendel, G., Paschmann, G., Sonnerup, B. U. O., et al. (2000). Extended magnetic reconnection at the Earth's magnetopause from detection of bi-directional jets. *Nature*, 404(6780), 848–850. <https://doi.org/10.1038/35009050>



- Pi, G., Němeček, Z., Šafránková, J., Grygorov, K., & Shue, J.-H. (2018). Formation of the dayside magnetopause and its boundary layers under the radial IMF. *Journal of Geophysical Research: Space Physics*, 123(5), 3533–3547. <https://doi.org/10.1029/2018ja025199>
- Pi, G., Shue, J.-H., Grygorov, K., Li, H.-M., Němeček, Z., Šafránková, J., et al. (2017). Evolution of the magnetic field structure outside the magnetopause under radial IMF conditions. *Journal of Geophysical Research: Space Physics*, 122(4), 4051–4063. <https://doi.org/10.1002/2015JA021809>
- Plaschke, F., Hietala, H., Archer, M., Blanco-Cano, X., Kajdic, P., Karlsson, T., et al. (2018). Jets downstream of collisionless shocks. *Space Science Reviews*, 214(5), 81. <https://doi.org/10.1007/s11214-018-0516-3>
- Pollock, C., Moore, T., Jacques, A., Burch, J., Gliese, U., Saito, Y., et al. (2016). Fast plasma investigation for Magnetospheric Multiscale. *Space Science Reviews*, 199(1–4), 331–406. <https://doi.org/10.1007/s11214-016-0245-4>
- Reiff, P. H., Hill, T. W., & Burch, J. L. (1977). Solar wind plasma injections at the dayside magnetospheric cusp. *Journal of Geophysical Research*, 82(4), 479–491. <https://doi.org/10.1029/ja082i004p00479>
- Rosenbauer, H., Grünwaldt, H., Montgomery, M. D., Paschmann, G., & Sckopke, N. (1975). Heos 2 plasma observations in the distant polar magnetosphere: The plasma mantle. *Journal of Geophysical Research*, 80(19), 2723–2737. <https://doi.org/10.1029/ja080i019p02723>
- Russell, C. T. (2002). Multiscale coupling in planetary magnetospheres. *Advances in Space Research*, 30(12), 2647–2656. [https://doi.org/10.1016/S0273-1177\(02\)80372-6](https://doi.org/10.1016/S0273-1177(02)80372-6)
- Russell, C. T., Anderson, B. J., Baumjohann, W., Bromund, K. R., Dearborn, D., Fischer, D., et al. (2016). The Magnetospheric Multiscale magnetometers. *Space Science Reviews*, 199(1–4), 189–256. <https://doi.org/10.1007/s11214-014-0057-3>
- Russell, C. T., Luhmann, J. G., Odera, T. J., & Stuart, W. F. (1983). The rate of occurrence of dayside Pc 3,4 pulsations: The L-value dependence of the IMF cone angle effect. *Geophysical Research Letters*, 10(8), 663–666. <https://doi.org/10.1029/gl010i008p00663>
- Russell, C. T., Petrinec, S. M., Zhang, T. L., Song, P., & Kawano, H. (1997). The effect of foreshock on the motion of the dayside magnetopause. *Geophysical Research Letters*, 24(12), 1439–1441. <https://doi.org/10.1029/97gl01408>
- Šafránková, J., Hayosh, M., Gutynska, O., Němeček, Z., & Prech, L. (2009). Reliability of prediction of the magnetosheath  $B_z$  component from interplanetary magnetic field observations. *Journal of Geophysical Research*, 114(A12), A12213. <https://doi.org/10.1029/2009JA014552>
- Sawyer, R. P., Fuselier, S. A., Mukherjee, J., & Petrinec, S. M. (2019). An investigation of flow shear and diamagnetic drift effects on magnetic reconnection at Saturn's dawnside magnetopause. *Journal of Geophysical Research: Space Physics*, 124(11), 8457–8473. <https://doi.org/10.1029/2019JA026696>
- Schwartz, S. J., Burgess, D., & Moses, J. J. (1996). Low-frequency waves in the Earth's magnetosheath: Present status. *Annales de Geophysique*, 14(11), 1134–1150. <https://doi.org/10.1007/s005850050376>
- Scurry, L., & Russell, C. T. (1991). Proxy studies of energy transfer to the magnetosphere. *Journal of Geophysical Research*, 96(A6), 9541–9548. <https://doi.org/10.1029/91JA00569>
- Scurry, L., Russell, C. T., & Gosling, J. T. (1994). A statistical study of accelerated flow events at the dayside magnetopause. *Journal of Geophysical Research*, 99(A8), 14815–14829. <https://doi.org/10.1029/94ja00793>
- Shelley, E. G., Sharp, R. D., & Johnson, R. G. (1976).  $\text{He}^{++}$  and  $\text{H}^+$  flux measurements in the day side cusp: Estimates of convection electric field. *Journal of Geophysical Research*, 81(13), 2363–2370. <https://doi.org/10.1029/ja081i013p02363>
- Shevryev, N. N., Zastenker, G. N., Nozrachev, M. N., Němeček, Z., Šafránková, J., & Richardson, J. D. (2003). High and low frequency large amplitude variations of plasma and magnetic field in the magnetosheath: Radial profile and some features. *Advances in Space Research*, 31(5), 1389–1394. [https://doi.org/10.1016/s0273-1177\(03\)00008-5](https://doi.org/10.1016/s0273-1177(03)00008-5)
- Shue, J.-H., Chao, J.-K., Song, P., McFadden, J. P., Suvorova, A., Angelopoulos, V., et al. (2009). Anomalous magnetosheath flows and distorted subsolar magnetopause for radial interplanetary magnetic fields. *Geophysical Research Letters*, 36(18), L18112. <https://doi.org/10.1029/2009GL039842>
- Sibeck, D. G. (1992). Transient events in the outer magnetosphere: Boundary waves or FTEs? *Journal of Geophysical Research*, 97(A4), 4009. <https://doi.org/10.1029/91ja03017>
- Smith, M. F., & Lockwood, M. (1996). Earth's magnetospheric cusp. *Reviews of Geophysics*, 34(2), 233–260. <https://doi.org/10.1029/96rg00893>
- Song, P., Elphic, R. C., & Russell, C. T. (1988). ISEE-1 and -2 observations of the oscillating magnetopause. *Geophysical Research Letters*, 15(8), 744–747. <https://doi.org/10.1029/gl015i008p00744>
- Song, P., Russell, C. T., & Gary, S. P. (1994). Identification of low-frequency fluctuations in the terrestrial magnetosheath. *Journal of Geophysical Research*, 99(A4), 6011–6025. <https://doi.org/10.1029/93JA03300>
- Song, P., Russell, C. T., & Huang, C. Y. (1993). Wave properties near the subsolar magnetopause: Pc 1 waves in the sheath transition layer. *Journal of Geophysical Research*, 98(A4), 5907–5924. <https://doi.org/10.1029/92JA02343>
- Song, P., Russell, C. T., & Thomsen, M. F. (1992). Waves in the inner magnetosheath: A case study. *Geophysical Research Letters*, 19(22), 2191–2194. <https://doi.org/10.1029/92GL02499>
- Sonnerup, B. U. Ö., Paschmann, G., Papamastorakis, I., Sckopke, N., Haerendel, G., Bame, S. J., et al. (1981). Evidence for magnetic field reconnection at the Earth's magnetopause. *Journal of Geophysical Research*, 86(A12), 10049–10067. <https://doi.org/10.1029/ja086ia12p10049>
- Swisdak, M., Rogers, B. N., Drake, J. F., & Shay, M. A. (2003). Diamagnetic suppression of component magnetic reconnection at the magnetopause. *Journal of Geophysical Research*, 108(A5), 1218. <https://doi.org/10.1029/2002JA009726>
- Takagi, K., Hashimoto, C., Hasegawa, H., Fujimoto, M., & TanDokor, R. (2006). Kelvin-Helmholtz instability in a magnetotail flank-like geometry: Three-dimensional MHD simulations. *Journal of Geophysical Research*, 111(A8), A08202. <https://doi.org/10.1029/2006JA011631>
- Tang, B. B., Wang, C., & Li, W. Y. (2013). The magnetosphere under the radial interplanetary magnetic field: A numerical study. *Journal of Geophysical Research: Space Physics*, 118(12), 7674–7682. <https://doi.org/10.1002/2013JA019155>
- Torbert, R. B., Russell, C. T., Magnes, W., Ergun, R. E., Lindqvist, P. A., LeContel, O., et al. (2016). The FIELDs instrument suite on MMS: Scientific objectives, measurements, and data products. *Space Science Reviews*, 199(1–4), 105–135. <https://doi.org/10.1007/s11214-014-0109-8>
- Trattner, K. J., Burch, J. L., Ergun, R., Eriksson, S., Fuselier, S. A., Giles, B. L., et al. (2017). The MMS dayside reconnection locations during Phase 1 and their relation to the predictions of the maximum magnetic shear model. *Journal of Geophysical Research: Space Physics*, 122(12), 11991–12005. <https://doi.org/10.1002/2017JA024488>
- Trattner, K. J., Burch, J. L., Ergun, R., Eriksson, S., Fuselier, S. A., Giles, B. L., et al. (2018). The transition between anti-parallel and component magnetic reconnection at the Earth's dayside magnetopause. *Journal of Geophysical Research: Space Physics*, 123(12), 10177–10188. <https://doi.org/10.1029/2018JA026081>
- Trattner, K. J., Burch, J. L., Fuselier, S. A., Petrinec, S. M., & Vines, S. K. (2020). The November 18 2015 magnetopause crossing: The GEM dayside kinetic challenge event observed by MMS/HPCA. *Journal of Geophysical Research: Space Physics*, 125(7), e2019JA027617. <https://doi.org/10.1029/2019JA027617>
- Trattner, K. J., Coates, A. J., Fazakerley, A. N., Johnstone, A. D., Balsiger, H., Burch, J. L., et al. (1998). Overlapping ion events in the cusp: Polar/TIMAS results. *Geophysical Research Letters*, 25(10), 1612–1624. <https://doi.org/10.1029/98gl01060>

- Trattner, K. J., Fuselier, S. A., Peterson, W. K., Sauvaud, J. A., Stenuit, H., Dubouloz, N., & Kovrazhkin, R. A. (1999). On spatial and temporal structures in the cusp. *Journal of Geophysical Research*, 104(A12), 28411–28421. <https://doi.org/10.1029/1999ja900419>
- Trattner, K. J., Fuselier, S. A., Petrinec, S. M., Burch, J. L., Ergun, R. R., & Grimes, E. W. (2021). Long and active magnetopause reconnection X-lines during changing IMF conditions. *Journal of Geophysical Research: Space Physics*, 125(4), e2020JA028926. <https://doi.org/10.1029/2020JA028926>
- Trattner, K. J., Fuselier, S. A., Petrinec, S. M., Yeoman, T. K., Mouikis, C., Kucharek, H., & Rème, H. (2005). The reconnection sites of spatial cusp structures. *Journal of Geophysical Research*, 110(A4), A04207. <https://doi.org/10.1029/2004JA010722>
- Trattner, K. J., Mulcock, J. S., Petrinec, S. M., & Fuselier, S. A. (2007). Probing the boundary between anti-parallel and component reconnection during southward interplanetary magnetic field conditions. *Journal of Geophysical Research*, 112(A8), A08210. <https://doi.org/10.1029/2007JA012270>
- Trattner, K. J., Petrinec, S. M., & Fuselier, S. A. (2021). The location of magnetic reconnection at Earth's magnetopause. *Space Science Reviews*, 217(41), 1–47. <https://doi.org/10.1007/s11214-021-00817-8>
- Trattner, K. J., Petrinec, S. M., Fuselier, S. A., Omid, N., & Sibeck, D. G. (2012). Evidence of multiple reconnection lines at the magnetopause from cusp observations. *Journal of Geophysical Research*, 117(A1), A01213. <https://doi.org/10.1029/2011JA017080>
- Trenchi, L., Marcucci, M. F., Pallochia, G., Consolini, G., Bavassano Cattaneo, M. B., Di Lellis, A. M., et al. (2008). Occurrence of reconnection jets at the dayside magnetopause: Double Star observations. *Journal of Geophysical Research*, 113(A7), A07S10. <https://doi.org/10.1029/2007JA012774>
- Vines, S. K., Fuselier, S. A., Trattner, K. J., Petrinec, S. M., & Drake, J. F. (2015). Ion acceleration dependence on magnetic shear angle in dayside magnetopause reconnection. *Journal of Geophysical Research: Space Physics*, 120(9), 7255–7269. <https://doi.org/10.1002/2015JA021464>
- Webster, J. M., Burch, J. L., Reiff, P. H., Daou, A. G., Genestreti, K. J., Graham, D. B., et al. (2018). Magnetospheric Multiscale dayside reconnection electron diffusion region events. *Journal of Geophysical Research: Space Physics*, 123(6), 4858–4878. <https://doi.org/10.1029/2018JA025245>
- Zhang, T. L., Zhao, H., Russell, C. T., Petrinec, S. M., Schwingenschuh, K., & Riedler, W. (1997). Dayside reconnection during IMF northward: A possible foreshock effect. *Advances in Space Research*, 19(12), 1943–1946. [https://doi.org/10.1016/S0273-1177\(97\)00106-3](https://doi.org/10.1016/S0273-1177(97)00106-3)
- Zhao, C. (2019). *Statistical study on two types of flux transfer events observed by MMS spacecraft*. UCLA. Retrieved from <http://dissertations.umi.com/ucla/17883>. <https://escholarship.org/uc/item/5jb369td>